Acta Crystallographica Section F
Structural Biology and Crystallization Communications
ISSN 1744-3091

Purification, crystallization and preliminary data analysis of ligand–receptor complexes of growth and differentiation factor 5 (GDF5) and BMP receptor IB (BRIB)

Alexander Kotzsch,[a] Joachim Nickel,[b] Walter Sebald[b] and Thomas D. Mueller[a]*

[a]Lehrstuhl für Botanik I – Molekulare Pflanzenphysiologie und Biophysik, Julius-von-Sachs-Institut für Biowissenschaften (Biozentrum) der Universität Würzburg, Julius-von-Sachs-Platz 2, D-97082 Würzburg, Germany, and [b]Lehrstuhl für Physiologische Chemie II, Theodor-Boveri-Institut für Biowissenschaften (Biozentrum) der Universität Würzburg, Am Hubland, D-97074 Würzburg, Germany

Correspondence e-mail: mueller@botanik.uni-wuerzburg.de

Received 18 May 2008
Accepted 24 June 2009

The ligand–receptor complex of GDF5 bound to its type I and type II receptors BRIB and ActRIIB was produced and crystallized. Crystals of the GDF5–BRIB complex could only be obtained if a ternary complex comprising GDF5, BRIB and the extracellular domain of the type II receptor ActRIIB was used in crystallization; however, the type II receptor ActRIIB was lost during crystallization. Crystals of this complex belonged to the tetragonal space group $P4_22_12$, with unit-cell parameters $a = b = 76.46$, $c = 82.78$ Å. Small changes in the crystallization condition resulted in crystals with a different morphology. These crystals consisted of the full ternary complex GDF5–BRIB–ActRIIB, but only diffracted to low resolution.

1. Introduction

Growth and differentiation factor 5 (GDF5) and bone morphogenetic protein 2 (BMP2), which are members of the transforming growth factor (TGF-β) superfamily of secreted cytokines, exhibit important functions in the development of the skeleton (Storm & Kingsley, 1996; Francis-West *et al.*, 1999). BMPs and GDFs signal *via* ligand-induced oligomerization of single transmembrane serine/threonine receptor kinases designated type I and type II receptors (Heldin *et al.*, 1997; Massague, 1998). Upon assembly of a heterohexameric complex comprising the dimeric ligand and two type I receptors as well as two type II receptors, an intracellular phosphorylation cascade activates SMAD proteins, which regulate the transcription of target genes in the cell nucleus (Heldin *et al.*, 1997; Massague, 1998).

Although the structures of BMP2 and GDF5 seem to be highly similar and the type I receptor epitopes of both ligands share several conserved residues, the binding of the two ligands to BMP receptor IA (BRIA) and BMP receptor IB (BRIB) differs (Nickel *et al.*, 2005). While BMP2 binds both type I receptors with almost identical affinities, the interaction of GDF5 with BRIA occurs with about 20-fold lower affinity compared with binding to BRIB. Thus, differences in the architecture and composition of the type I binding epitope in GDF5 and BMP2 must be responsible for the different binding specificity.

In order to understand the molecular basis of how GDF5 can generate specificity towards its type I receptor BRIB, we aimed towards structural analysis of GDF5–type I receptor complexes. Here, we demonstrate that the extracellular domain (EC) of a type II receptor, ActRIIB, can act in an additive/chaperone-like manner, thereby facilitating crystallization of the binary complex of GDF5 bound to BRIB. Further investigation revealed that by varying the crystallization conditions crystals consisting of either the binary complex GDF5–$BRIB_{EC}$ or the full ternary complex GDF5–$BRIB_{EC}$–$ActRIIB_{EC}$ can be obtained.

2. Materials and methods

2.1. Protein expression and purification

The extracellular domain of murine BRIB ($BRIB_{EC}$; residues 14–126; Swiss-Prot P36898) was expressed as a thioredoxin fusion in the cytoplasm of *Escherichia coli* strain AD494 (DE3), similar to the

protocol described for the BMP type I receptor BMPR-IA (Kirsch *et al.*, 2000). On reaching an optical density of 0.6 at 600 nm, the cells were cooled to 293 K and expression of Trx-$BRIB_{EC}$ was initiated with 1 m*M* IPTG and continued at 293 K overnight.

Cells were harvested, resuspended in 20 m*M* Tris pH 7.9, 500 m*M* NaCl, 20 m*M* imidazole and lysed by sonication. The supernatant was clarified by centrifugation and subjected to metal-ion affinity chromatography using Ni^{2+}–NTA resin. The protein was eluted using 500 m*M* imidazole and cleaved using 0.3 U thrombin (Sigma) per milligram of Trx-$BRIB_{EC}$. Thioredoxin, monomeric and multimeric $BRIB_{EC}$ were separated by gel filtration. Residual traces of thioredoxin were depleted by a second metal-ion affinity chromatography step. For final purification, $BRIB_{EC}$ protein was subjected to affinity chromatography using a BMP2 affinity matrix. Only 15–20% of the $BRIB_{EC}$ could be bound and recovered, showing that the majority of the BRIB protein was inactive. The final yield of monomeric active $BRIB_{EC}$ was roughly 0.4 mg per gram of cell pellet.

The extracellular domain of the activin type II receptor ActRIIB ($ActRIIB_{EC}$) was prepared as a thioredoxin-fusion protein as described previously (Weber *et al.*, 2007). The mature part of human GDF5 (residues 381–501; Swiss-Prot 43206) was expressed in *E. coli*, isolated from inclusion bodies, refolded and purified to homogeneity as described previously (Mueller *et al.*, 2005). Selenomethionine (SeMet) labelled GDF5 was produced using the methionine-auxotroph *E. coli* strain B834 (DE3) similarly to as in previously published protocols (Budisa *et al.*, 1995).

2.2. Preparation and crystallization of the ligand–receptor complexes

The complex of GDF5 bound to $BRIB_{EC}$ and $ActRIIB_{EC}$ was obtained *via* a two-step procedure. Firstly, the binary complex of GDF5 and two molar equivalents of $BRIB_{EC}$ was prepared. GDF5 was dissolved in water to a concentration of 5 µ*M* and $BRIB_{EC}$ was dissolved in buffer containing 20 m*M* HEPES pH 7.4 and 1 *M* NaCl to a concentration of 11 µ*M*. Equal amounts of the two protein solutions were mixed, yielding a molar ratio of 1:2.2. The complex was incubated for 20 min at 294 K and applied to gel filtration using HBS_{500} buffer (10 m*M* HEPES pH 7.4, 500 m*M* NaCl). The ternary complex comprising GDF5, $BRIB_{EC}$ and $ActRIIB_{EC}$ was then prepared by adding a 2.2-fold molar amount of $ActRIIB_{EC}$ to this binary complex. The mixture was incubated for 20 min and subjected to gel filtration as above. Fractions containing the GDF5–$BRIB_{EC}$–$ActRIIB_{EC}$ complex were concentrated to 5 mg ml^{-1} for crystallization.

Since diffracting crystals of the binary GDF5–$BRIB_{EC}$ complex could not be obtained, crystallization of the ternary complex GDF5–$BRIB_{EC}$–$ActRIIB_{EC}$ was performed instead. Sparse-matrix screening yielded three conditions that produced single crystals (Hampton Crystal Screen Cryo No. 28, PEG/Ion Screen No. 20 and Index Screen No. 58). During fine screening, we observed two different crystal forms that exhibited either an octahedron-like or a blade-like morphology depending on the presence of either polyethylene glycol (PEG) or polypropylene glycol (PPG) (Figs. 1*a* and 1*b*). Crystals with blade-like morphology that reached dimensions of 150 × 40 × 40 µm were obtained within 5 d at 294 K from 0.1 *M* bis-tris pH 5.5, 50%(*v*/*v*) PPG 400. These crystals diffracted to 3.2 Å resolution. The resolution limits could be improved by replacing the bis-tris with sodium acetate and adding Mg^{2+} at a concentration between 30 and 50 m*M* and DMSO at a concentration of 5%(*v*/*v*). For data acquisition, crystals were grown from 0.1 *M* sodium acetate pH 5.3, 50%(*v*/*v*) PPG 400, 30 m*M* $MgSO_4$. SeMet-labelled crystals with blade-like morphology were grown at 294 K by mixing 1 µl SeMet GDF5–$BRIB_{EC}$–$ActRIIB_{EC}$ solution (3 mg ml^{-1}) in HBS_{500} buffer with 1 µl

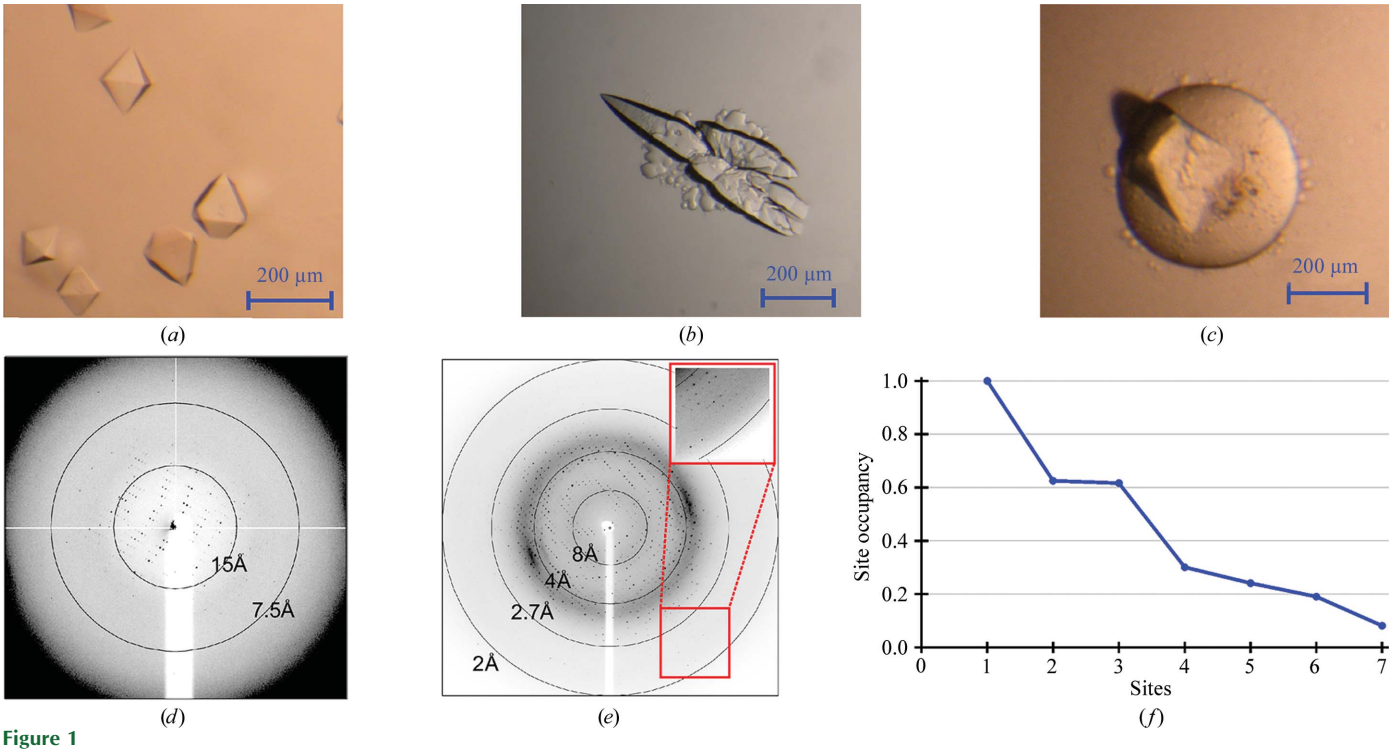

Figure 1
(*a*) Octahedron-like crystals with dimensions of 40 × 40 × 40 µm. (*b*) Blade-like crystals consisting of the GDF5–$BRIB_{EC}$ complex. The crystals grew to dimensions of 100 × 50 × 50 µm within 5 d. (*c*) SeMet-labelled blade-like crystal consisting of the GDF5–$BRIB_{EC}$ complex. (*d*, *e*) Diffraction patterns and diffraction limits of the crystals in (*b*) and (*a*), respectively. (*f*) Selenium sites in the SeMet-labelled blade-like crystals in (*c*) consisting of the GDF5–$BRIB_{EC}$ complex. Three of five sites could be refined with *SHARP*.

Table 1
Data-collection and processing statistics for the native crystals of GDF5–$BRIB_{EC}$ and GDF5–$BRIB_{EC}$–$ActRIIB_{EC}$.

Values in parentheses are for the highest resolution shell.

	Native blade-like crystal	Native octahedron-like crystal
Beamline	SLS, X06SA	ESRF, ID23-2
Detector	MAR 225 Mosaic	MAR 225 Mosaic
Space group	$P4_22_12$	$P4_1$
Temperature (K)	100	100
Unit-cell parameters (Å, °)	$a = b = 76.46$, $c = 82.76$, $\alpha = \beta = \gamma = 90$	$a = b = 125.77$, $c = 201.40$, $\alpha = \beta = \gamma = 90$
Wavelength (Å)	1.1049	0.9340
Resolution (Å)	34.19–2.10 (2.18–2.10)	44.47–6.80 (7.04–6.80)
No. of reflections (total/unique)	144233/14815	30743/5420
Completeness (%)	99.5 (100)	99.9 (100)
Multiplicity	9.7 (9.9)	5.6 (5.7)
R_{merge}† (%)	7.1 (35.4)	12.9 (60.8)
$\langle I/\sigma(I)\rangle$	14.7 (5.3)	6.6 (2.1)
No. of molecules in ASU	1	3
Matthews coefficient (Å^3 Da^{-1})	2.3	3.4
Solvent content (%)	47.2	63.9

† $R_{merge} = \sum_{hkl}\sum_i |I_i(hkl) - \langle I(hkl)\rangle| / \sum_{hkl}\sum_i I_i(hkl)$, where $I_i(hkl)$ is the intensity of the ith observation of the unique reflection hkl; $\langle I(hkl)\rangle$ is the mean of the intensities of all observations of reflection hkl.

Table 2
Data-collection and processing statistics for the SeMet-labelled GDF5–$BRIB_{EC}$ crystal.

Values in parentheses are for the highest resolution shell.

Beamline	BESSY, BL14.1		
Detector	MAR 225 Mosaic		
Space group	$P4_22_12$		
Temperature (K)	100		
Unit-cell parameters (Å, °)	$a = b = 76.62$, $c = 82.12$, $\alpha = \beta = \gamma = 90$		
Wilson B factor (Å^2)	63.7		
Wavelength (Å)	0.97979	0.97962	0.90789
Resolution (Å)	36.32–2.90 (3.00–2.90)	38.31–2.60 (2.69–2.60)	36.26–2.90 (3.00–2.90)
No. of reflections (total/unique)	39424/5862	54117/7962	35898/5839
Completeness (%)	99.8 (100.0)	99.9 (100.0)	99.9 (100.0)
Multiplicity	6.69 (6.93)	6.75 (6.85)	6.10 (6.30)
R_{merge}† (%)	15.7 (49.2)	10.0 (40.8)	12.0 (39.0)
R_{anom}‡ (%)	5.6	5.7	5.3
$\langle I/\sigma(I)\rangle$	6.2 (2.5)	9.1 (3.5)	8.6 (3.7)
Phasing	3 of 5 selenium positions identified, three-wavelength MAD + native (*SHARP*)		
R_{Cullis}	0.85	0.66	0.89
R.m.s. lack of closure	0.87	1.12	0.89
Phasing power	0.71	1.82	0.53
Mean figure of merit	0.18		
Figure of merit after *DM*	0.83		

† $R_{merge} = \sum_{hkl}\sum_i |I_i(hkl) - \langle I(hkl)\rangle| / \sum_{hkl}\sum_i I_i(hkl)$, where $I_i(hkl)$ is the intensity of the ith observation of the unique reflection hkl; $\langle I(hkl)\rangle$ is the mean of the intensities of all observations of reflection hkl. ‡ $R_{anom} = \sum_{hkl}(\langle I^+\rangle - \langle I^-\rangle) / \sum_{hkl}(\langle I^+\rangle_i I^-\rangle)$.

0.1 *M* sodium acetate pH 5.3, 50% PPG 400, 50 m*M* magnesium formate and placing the drop over a 1 ml reservoir of the latter solution. Octahedron-like crystals of dimensions 40 × 40 × 40 µm grew within 11 d at 294 K in hanging drops consisting of 1 µl protein solution and 1 µl 0.085 *M* sodium cacodylate pH 6.5, 25.5%(*w*/*v*) PEG 8000, 0.13 *M* sodium acetate, 15%(*v*/*v*) glycerol; the drops were placed over a 1 ml reservoir of 0.085 *M* sodium cacodylate pH 6.5, 25.5%(*w*/*v*) PEG 8000, 0.13 *M* sodium acetate, 15%(*v*/*v*) glycerol.

2.3. Data collection

Data from the blade-like crystals were collected on beamline XS06 at the Swiss Light Source (Villigen, Switzerland). The crystals were directly flash-frozen in liquid nitrogen. The crystal-to-detector distance was set to 180 mm, the wavelength was 1.10485 Å and data collection was performed at 100 K, rotating the crystal through 125° (1° oscillations) with 2 s exposure per frame. Multiple anomalous dispersion (MAD) data sets for experimental phasing were acquired at 100 K on beamline BL14.2 at BESSY (Berlin) at three wavelengths. The crystal-to-detector distance was 190 mm and crystals were rotated through a total of 90°, with 1° oscillation and an exposure of 3 s per frame. Data from the crystals with octahedron-like morphology were acquired on beamline ID23-2 at the ESRF (Grenoble) at 100 K. Crystals were rotated through 146° (1° oscillation); the wavelength was 0.9340 Å and the crystal-to-detector distance was set to 324 mm. Data processing was accomplished using the software *CrystalClear* (Rigaku MSC), *SHELXC*/*D*/*E* (Sheldrick, 2008) and *SHARP*/*AutoSHARP* v.2.2.0 (Bricogne *et al.*, 2003).

3. Results and discussion

3.1. Crystallization of the GDF5–$BRIB_{EC}$–$ActRIIB_{EC}$ complex and data processing

Initial sparse-matrix crystallization screens employing a protein solution consisting of the GDF5–$BRIB_{EC}$–$ActRIIB_{EC}$ complex yielded two conditions giving rise to crystals of different (blade-like or octahedron-like) morphology. The diffraction of the blade-like crystals could be significantly improved by additive screening, with 30–50 m*M* Mg^{2+} as well as 5% DMSO shifting the diffraction limit to 2.0 Å (Fig. 1*d*). In contrast, the octahedron-like crystals could be improved in terms of size but their diffraction remained at 6.5–6.8 Å (Fig. 1*e*). Complete data sets were obtained from native and SeMet-labelled blade-like and octahedron-like crystals at synchrotron sources. Native data from the blade-like crystals could be processed to a resolution of 2.1 Å, MAD data from the blade-like crystals to 2.6 Å resolution and native data from the octahedron-like crystals to a resolution of 6.8 Å (Tables 1 and 2). Both native and SeMet-labelled crystals with blade-like morphology belonged to space group $P4_22_12$, with a relatively small unit cell (Tables 1 and 2). The lattice symmetry of the crystals with octahedron-like morphology also suggested a tetragonal space group, either $P4_1$ or $P4_3$. However, the unit cell is much larger (Table 1).

3.2. Data analysis of the two crystal forms

Both the blade-like and octahedron-like crystals were analyzed by SDS–PAGE and Western blotting. The octahedron-like crystals contained all the protein components of the initial crystallization setup (Fig. 2*a*). In contrast, only GDF5 and $BRIB_{EC}$ were present in the blade-like crystals. Calculation of the Matthews coefficient suggested the presence of one GDF5 monomer and one $BRIB_{EC}$ molecule in the asymmetric unit of the blade-like crystals. For the SeMet-labelled crystals, three of the five Se-atom positions originating from five methionine residues in the GDF5 monomer could be identified using *SHELX* and *SHARP*/*autoSHARP* (Fig. 1*f*). Structure analysis confirmed that the crystals exhibiting the blade-like morphology indeed consisted of only GDF5 and the type I receptor $BRIB_{EC}$. The structure of the binary complex GDF5–$BRIB_{EC}$ has now been solved and refined to high resolution (PDB entry 3evs; Kotzsch *et al.*, 2009). A symmetry-related BRIB molecule forming the crystal lattice blocks the putative position of $ActRIIB_{EC}$ expected in a ternary complex. The type II receptor $ActRIIB_{EC}$, which is part of the ternary complex isolated by gel filtration, is lost during crystallization.

The low-resolution 6.8 Å data set acquired from an octahedron-like crystal was analyzed by molecular replacement using the software *Phaser* v.1.3 (McCoy *et al.*, 2007). The ternary complex BMP2–$BRIA_{EC}$–$ActRIIB_{EC}$ (PDB code 2h62; Weber *et al.*, 2007) as well as

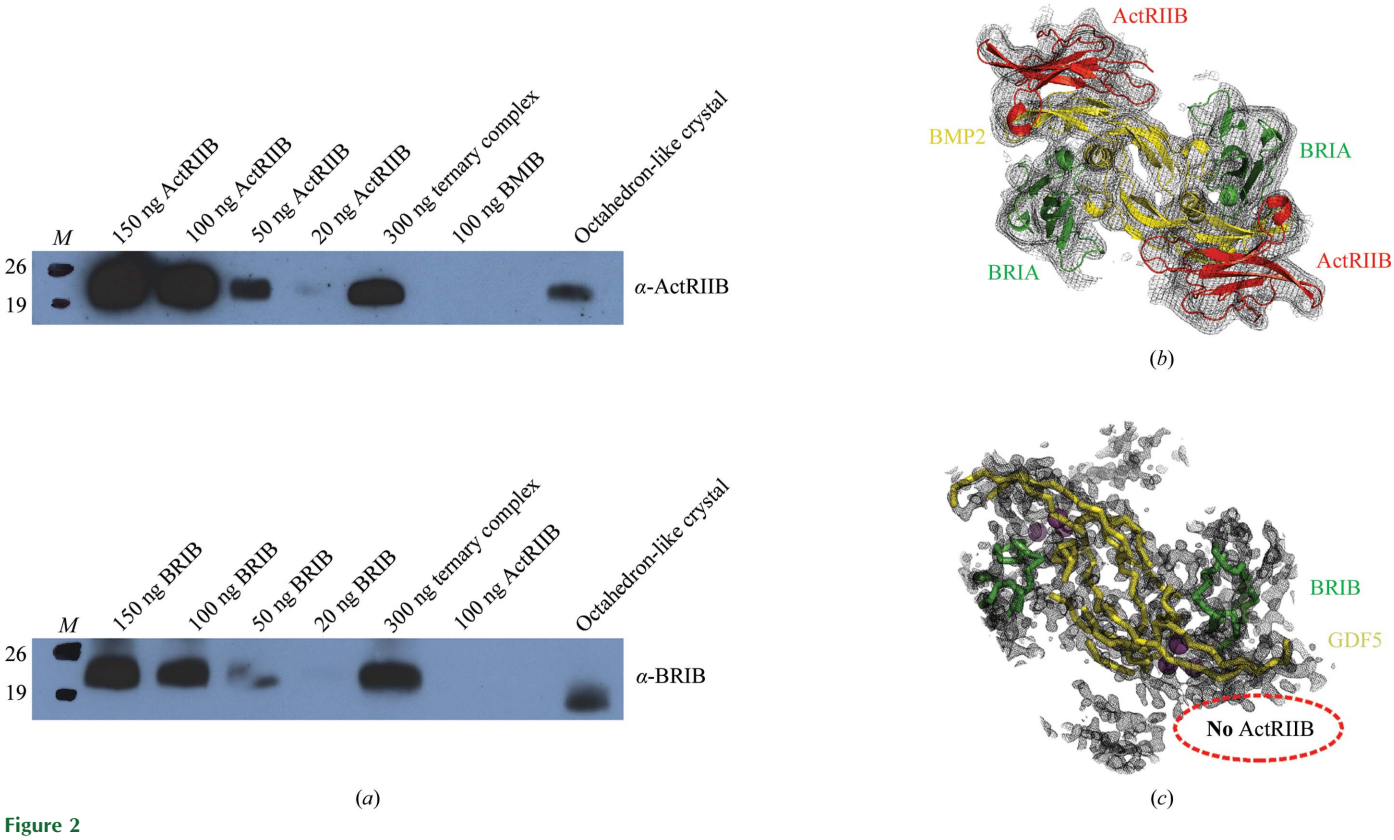

Figure 2
(*a*) Western blotting analysis of octahedron-like crystals. Crystals were washed, analyzed by SDS–PAGE and blotted onto nitrocellulose. The membrane was incubated first with α-BRIB (goat, 1:500; Santa Cruz) or α-ActRIIB (rabbit, 1:2000; Immunoglobe) antibodies and then with HRP-coupled α-goat-IgG (1:8000; Santa Cruz) or α-rabbit-IgG (1:1000; Rockland), respectively. Staining was performed using SuperSignal West Pico Chemiluminescent Substrate (Pierce). (*b*) Electron density for octahedron-like crystals calculated from the molecular-replacement solution. The search model is fitted into the electron density, showing that all three components are present forming the heterohexameric complex. (*c*) Initial electron-density map ($2F_{obs} - F_{calc}$) for blade-like crystals (comprising SeMet GDF5) after *autoSHARP* and density modification using *DM* (contour level 1σ). An automated tracing using *ARP*/*wARP* is shown as a yellow (GDF5) and green (BRIB) C^{α} trace. A red stippled circle marks the position of the expected $ActRIIB_{EC}$.

the binary complex BMP2–$BRIA_{EC}$ (PDB code 1rew; Keller *et al.*, 2004) were used as search models. Calculation of the Matthews coefficient (Matthews, 1968) suggested the presence of three GDF5–$BRIB_{EC}$–$ActRIIB_{EC}$ ternary complexes (molecular weight ∼78 kDa) in the asymmetric unit ($V_M = 3.4$ Å^3 Da^{-1}). Searching with the binary complex BMP2–$BRIA_{EC}$ yielded a lattice lacking crystal contacts and showing large gaps between accompanying complexes. This confirms the Western blot analysis, which suggested the presence of the type II receptor ActRIIB in these crystals. Using the ternary complex BMP2–$BRIA_{EC}$–$ActRIIB_{EC}$ (PDB code 2h62; Weber *et al.*, 2007) in the rotational and translational search, a clear unambiguous solution for a full ternary complex assembly could be obtained.

Calculation of a $2F_{obs} - F_{calc}$ electron-density map using the molecular-replacement solution for phasing showed clear although bulky electron density for the ternary complex comprising the ligand dimer, two type I and two type II receptors in the asymmetric unit. Further analysis was impeded by the low resolution, but the observation that all components of the ternary complex are fully covered by electron density confirmed the Western blotting analysis of this crystal form (Fig. 2*a*). Thus, the seemingly small differences in crystallization conditions leading to these two different crystal forms, 50% PPG 400 at pH 5.3 *versus* 25% PEG 8000 at pH 6.5, is likely to account for the formation/stabilization of the two different assemblies in the crystals.

This is interesting as the same protein complex isolated from gel filtration was used in the two crystallization setups. At high concentrations of PPG 400 $ActRIIB_{EC}$ seems to dissociate from the complex and thus only the remaining binary complex is observed in the crystal lattice. It is especially noteworthy that crystallization experiments employing only the binary complex GDF5–$BRIB_{EC}$ and the same crystallization conditions as described above were not successful. Also, performing larger screening trials using the binary complex GDF5–$BRIB_{EC}$ did not result in crystals that diffracted to a resolution better than 15 Å. This suggests that the $ActRIIB_{EC}$ protein, although not present in the resulting crystal lattice, is required for crystallization of the binary complex GDF5–$BRIB_{EC}$. Thus, $ActRIIB_{EC}$ might in this case be considered as an additive or chaperone in the crystallization of the binary complex of GDF5 bound to $BRIB_{EC}$.

Since it is important to know whether the binding of the activin type II receptor to the binary complex GDF5–$BRIB_{EC}$ complex results in a conformational change which could modulate signal transduction, improvement of the octahedron-shaped crystals is needed. Thus, further screening of additives and buffer chemistry will be performed.

This research was supported by the Deutsche Forschungsgemeinschaft SFB 487 B2. The authors gratefully acknowledge access to synchrotron beamlines BL14.2 at BESSY (Berlin), X06SA at SLS (Villigen) and ID23-2 at ESRF (Grenoble). We thank Clemens

Grimm for help in acquisition of the data set for the GDF5–BRIB$_{EC}$–ActRIIB$_{EC}$ complex.

References

Bricogne, G., Vonrhein, C., Flensburg, C., Schiltz, M. & Paciorek, W. (2003). *Acta Cryst.* D**59**, 2023–2030.

Budisa, N., Steipe, B., Demange, P., Eckerskorn, C., Kellermann, J. & Huber, R. (1995). *Eur. J. Biochem.* **230**, 788–796.

Francis-West, P. H., Abdelfattah, A., Chen, P., Allen, C., Parish, J., Ladher, R., Allen, S., MacPherson, S., Luyten, F. P. & Archer, C. W. (1999). *Development*, **126**, 1305–1315.

Heldin, C. H., Miyazono, K. & ten Dijke, P. (1997). *Nature (London)*, **390**, 465–471.

Keller, S., Nickel, J., Zhang, J. L., Sebald, W. & Mueller, T. D. (2004). *Nature Struct. Mol. Biol.* **11**, 481–488.

Kirsch, T., Nickel, J. & Sebald, W. (2000). *FEBS Lett.* **468**, 215–219.

Kotzsch, A., Nickel, J., Seher, A., Sebald, W. & Muller, T. D. (2009). *EMBO J.* **28**, 937–947.

Massague, J. (1998). *Annu. Rev. Biochem.* **67**, 753–791.

Matthews, B. W. (1968). *J. Mol. Biol.* **33**, 491–497.

McCoy, A. J., Grosse-Kunstleve, R. W., Adams, P. D., Winn, M. D., Storoni, L. C. & Read, R. J. (2007). *J. Appl. Cryst.* **40**, 658–674.

Mueller, T. D., Gottermeier, M., Sebald, W. & Nickel, J. (2005). *Acta Cryst.* F**61**, 134–136.

Nickel, J., Kotzsch, A., Sebald, W. & Mueller, T. D. (2005). *J. Mol. Biol.* **349**, 933–947.

Sheldrick, G. M. (2008). *Acta Cryst.* A**64**, 112–122.

Storm, E. E. & Kingsley, D. M. (1996). *Development*, **122**, 3969–3979.

Weber, D., Kotzsch, A., Nickel, J., Harth, S., Seher, A., Mueller, U., Sebald, W. & Mueller, T. D. (2007). *BMC Struct. Biol.* **7**, 6.